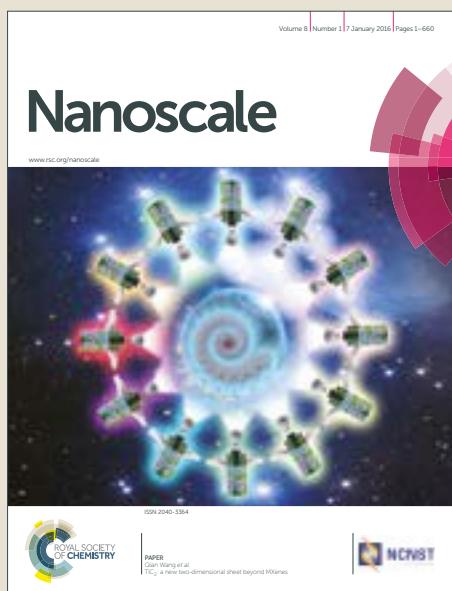


Nanoscale

Accepted Manuscript



This article can be cited before page numbers have been issued, to do this please use: Y. Wang, Y. Tang, P. Cheng, X. Zhou, Z. Zhu, Z. Liu, D. Liu, Z. M. Wang and J. Bao, *Nanoscale*, 2017, DOI: 10.1039/C6NR08487G.



This is an Accepted Manuscript, which has been through the Royal Society of Chemistry peer review process and has been accepted for publication.

Accepted Manuscripts are published online shortly after acceptance, before technical editing, formatting and proof reading. Using this free service, authors can make their results available to the community, in citable form, before we publish the edited article. We will replace this Accepted Manuscript with the edited and formatted Advance Article as soon as it is available.

You can find more information about Accepted Manuscripts in the [author guidelines](#).

Please note that technical editing may introduce minor changes to the text and/or graphics, which may alter content. The journal's standard [Terms & Conditions](#) and the ethical guidelines, outlined in our [author and reviewer resource centre](#), still apply. In no event shall the Royal Society of Chemistry be held responsible for any errors or omissions in this Accepted Manuscript or any consequences arising from the use of any information it contains.

Distinguishing Thermal Lens Effect from Electronic Third-order Nonlinear Self-phase Modulation in Liquid Suspensions of 2D Nanomaterials

Yanan Wang^{1,2}, Yingjie Tang³, Peihong Cheng^{4,2}, Xufeng Zhou⁵, Zhuan Zhu², Zhaoping Liu⁵, Dong Liu³, Zhiming Wang^{*1} and Jiming Bao^{*2,1}

¹Institute of Fundamental and Frontier Sciences, University of Electronic Science and Technology of China, Chengdu, Sichuan 610054, China

²Department of Electrical and Computer Engineering
University of Houston, Houston, Texas 77204, USA

³Department of Mechanical Engineering
University of Houston, Houston, Texas 77204, USA

⁴School of Electronic and Information Engineering
Ningbo University of Technology, Ningbo, Zhejiang 315211, China

⁵Key Laboratory of Graphene Technologies and Applications of Zhejiang Province, Ningbo Institute of Materials Technology & Engineering, Chinese Academy of Sciences, Ningbo, Zhejiang 315201, China

Corresponding Authors

*E-mail: jbao@uh.edu.

*E-mail: zhmwang@uestc.edu.cn.

Nanoscale Accepted Manuscript

Abstract

The interaction of light with atomically thin nanomaterials has attracted enormous research interests in order to understand two-dimensional (2D) electron systems and develop novel opto-electronic devices. The observations of spatial self-phase modulation and the associated multiple diffraction ring patterns in liquid suspension of 2D nanomaterials are believed to be excellent examples of strong laser interaction with 2D nanomaterials and this phenomena has been attributed to their large electronic third-order susceptibilities. By performing a series of control experiments with liquid suspensions of graphene and graphene oxide flakes in different solvents at various temperatures under an increasing modulation frequency of laser illumination, we first show that the diffraction ring pattern has little dependence on the type of nanomaterial but strongly depends on the duration of laser illumination. Laser induced local refractive index change is then monitored by a weaker probe beam, resulting in the divergent diffraction of the probe beam that indicates a lower self-induced refractive index in the center of the pump laser beam than its peripheral: a clear signature for the thermal lens effect. Finally, we use computational fluid dynamics to simulate laser induced temperature and index changes of the suspensions. The evolution of diffraction rings is well correlated to the transient temperature distribution. Our understanding of complex laser interactions with nanomaterial suspensions and the associated thermal lens effect pave the way for further basic studies and fluid opto-electronic applications of 2D nanomaterials.

Keywords: liquid suspended 2D nanomaterials, thermal lens effect, spatial self-phase modulation, fluid opto-electronics.

1. INTRODUCTION

The exploration of light-matter interactions was greatly accelerated by the inventions of lasers in 1960s because of their high intensity and directionality and their temporal and spatial coherence. The measurement of refractive index of a slab of media through the transmission and reflection of a laser beam is a classic and simple experiment ¹. This method breaks down when multiple conical diffractions, instead of a single laser beam, emerge from the media. The split of a single laser spot into multiple concentric diffraction rings when viewed on a far-field screen is one of the earliest examples of strong light-matter interaction ². It is well known that diffraction rings are a result of spatial self-phase modulation (SSPM) associated with laser induced local refractive index change. However, as to the origin of change in refractive index, there are several competing theories. Thermal lens effect was the earliest proposed theory, which ascribes the change in refractive index of the media to its increasing temperature after absorbing the laser light ²⁻⁴. The nonlinear refractive index n_2 or third-order susceptibility $\chi^{(3)}$ of the media is another contending theory for SSPM ⁵⁻⁸. An additional theory postulated for refractive change is laser induced molecular reorientation or polymerization ⁹⁻¹². Although the thermal lens effect is a linear optical phenomenon in principle because the refractive index change is not directly induced by the electrical field of the laser through $\chi^{(3)}$, its dependence on the laser intensity is similar to those from other theories, making it difficult to be separated from various other effects.

Similar multiple diffraction ring patterns were recently observed in liquid suspensions of graphene ¹³⁻¹⁵, two-dimensional transition metal dichalcogenides (TMDs) ¹⁶⁻¹⁹, black phosphor ²⁰, and carbon nanotubes (CNTs) ²¹, and have been regarded as a manifestation of their intrinsically large $\chi^{(3)}$. Due to its high electron mobility and unique Dirac cone-like band

structure, graphene exhibits large electron polarization, giving rise to huge linear and nonlinear optical responses²². For instance, strong second harmonics generation, saturable absorbance, and four-wave mixing have been observed in atom-thick layers of graphene²³⁻²⁶. However, other mechanisms may equally contribute to the observed SSPM in liquid suspensions of graphene or other nanomaterials. In fact, the thermal lens effect has accounted for SSPM in solutions of many absorbing materials such as dye molecules and C₆₀^{27, 28}. Laser induced reorientation of 2D flakes is another possible cause of SSPM since liquid suspensions of 2D nanomaterials are essentially a new type of nematic liquid crystals^{9, 29-31}.

In this work, we first performed a series of control experiments with different nanomaterials, solvents, solvent temperatures, and modulation frequencies of laser intensity. A pump-probe method was then used to monitor the laser-induced change of spatial optical index of the dispersion. Finally, we employed computational fluid dynamics to obtain the evolution and distribution of temperature of dispersion and correlate it with the dynamics of diffraction ring pattern. Based on these observations and their good agreement with the simulation, we conclude that the observed ring pattern is a purely thermal lens effect of the dispersion and has nothing to do with the electronic nonlinear optical effect of 2D material. The role of nanomaterials is simply to absorb laser light and convert it into heat. Liquid suspensions of 1D or 2D materials provide innovative routes for basic study of light-matter interaction and photonic applications that cannot be achieved when they are in solid state³⁰⁻³⁹. Due to the extreme shape anisotropy of 1D or 2D nanomaterials, their liquid suspensions are inherently anisotropic in many aspects, ranging from their optical properties and thermophysical properties to fluidic transport characteristics^{35, 40, 41}. The determination of an underlying mechanism for SSPM and the effect of laser heating on the

dynamics of suspended 2D nanomaterials are essential to better understanding and potential fluid opto-electronic device applications of 2D nanomaterials.

2. MATERIALS AND METHODS

Graphene flakes were synthesized via intercalation and exfoliation of natural graphite by Ningbo Morsh Technology Co., Ltd. They are a few micrometers in lateral size and have an average thickness of 2.4 nm (7 layers), as can be seen from their scanning electron microscopy (SEM) and transmission electron microscopy (TEM) images in Fig. S1. Graphene oxide (GO) was prepared by a modified Hummers' method⁴². They are single-layer flakes with size in the range of 2-10 μm . Detailed synthesis steps and an atomic force microscopy (AFM) image (Fig. S2) can be found in the supplementary materials. Flakes of graphene or GO were then dispersed in N-Methyl-2-pyrrolidone (NMP), ethanol and de-ionized (DI) water. All sample solutions had concentrations in the range of 0.005-0.01% in weight (wt%), corresponding to 0.002-0.004% in volume fraction (vol%). The suspensions are kept at room temperature (25 °C) unless otherwise stated. To obtain the diffraction rings, a 532-nm continuous-wave (CW) laser was focused by a lens ($f = 100$ mm) on the suspensions of graphene or GO in a 10-mm cuvette. Unless otherwise stated, the concentration of graphene or GO is adjusted such that their optical transmission at 532 nm is kept nearly the same at 10-12%. A white screen was placed two meters away from the cuvette and far-field diffraction of the transmitted laser beam was recorded by a digital camera. Still images were created by extracting frames from video recordings. To modulate the intensity of the 532-nm laser, a mechanical chopper was used to turn the CW beam on and off at the frequencies of 20 Hz and 200 Hz with a 25% duty cycle. To probe the spatial refractive index

change induced by the 532-nm laser, a 633-nm 10-mW laser beam is launched perpendicularly to the 532-nm beam, and its transmitted light is imaged⁴³.

Numerical simulations were performed using the commercial computational fluid dynamics (CFD) software package Star-CCM+ to quantify the laser-heating induced temperature gradient. Since the beam path in the suspensions (10 mm) is much shorter than the 100-mm focal length, the laser beam was approximated as a collimated Gaussian beam with the diameter of 0.2 mm in the simulations. A 10 mm × 10 mm 2D domain perpendicular to the laser beam in the z direction was modeled. The Navier-Stokes equations and the energy equation were solved simultaneously to obtain the velocity and temperature fields. The absorption of incident laser beams by the graphene or GO flakes and the subsequent thermal transport to the ambient fluid are represented as a localized heat source in the domain center, defined as $Q(x, y) = \alpha I(x, y)$, $I(x, y) = \frac{2P}{\pi\rho^2} \exp\left(-\frac{2(x^2+y^2)}{\rho^2}\right)$, where α is the absorption coefficient, P is the incident laser power, and ρ is the diameter of the laser beam. Detailed parameters of the solvents for simulations, such as density, viscosity, specific heat and thermal conductivity, are included in the supporting materials.

3. RESULTS AND DISCUSSION

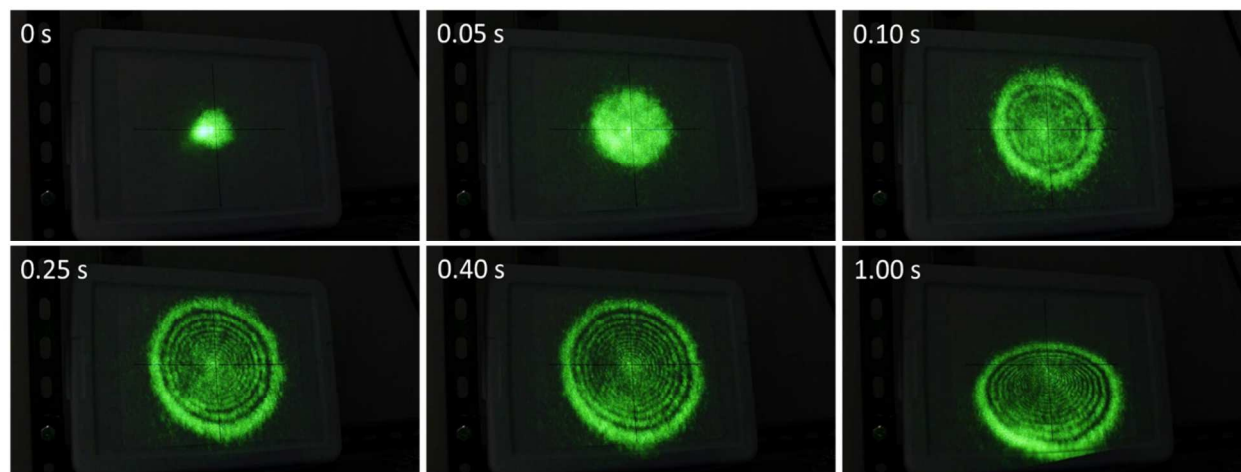


Figure 1. Typical time development of diffraction ring pattern of a continuous wave (532 nm) laser beam (60 mW) traversing a graphene suspension in NMP.

Figure 1 shows a typical example of a laser induced diffraction pattern in a graphene suspension. When the laser first passes through the suspension in a cuvette, an ordinary transmitted beam is observed with reduced intensity, but the laser spot of the transmitted beam begins to expand and the number of diffraction rings increase within milliseconds. The size of ring pattern reaches the maximum at ~ 0.4 seconds, and the ring pattern becomes squeezed in the vertical direction above the center of the beam and becomes stable after 1 second. Such a two-stage development is a general feature of previous observations in liquid suspensions of graphene and 2D TMDs^{13, 14, 16, 17}. The multiple diffraction rings clearly indicates a large phase shift experienced by the laser beam as each diffraction ring accounts approximately for a phase shift of 2π ⁹. Because the number of diffraction rings increases linearly with the laser intensity, these observations were attributed to the extraordinarily large $\chi^{(3)}$ of nearly all types of nanomaterials^{13-19, 21, 44}. The transient evolution of diffraction rings was believed to be caused by the spatial alignment of graphene flakes with the laser polarization^{13, 14}.

As mentioned earlier, the liquid suspension of graphene can exhibit a nematic phase; the multiple diffraction rings could be due to laser induced birefringence above the Fredericksz transition⁹. However, this mechanism can be excluded in this case because graphene flakes are not uniformly oriented initially due to the low concentration, and the dependence of the number of rings on laser power is linear without any apparent threshold (Fig. S3 and S4). Similar ring patterns have also been reported in solution of organic dye molecules, but were ascribed to the thermal lens effect of the solvent instead of $\chi^{(3)}$ of the molecules²⁷. In the following paragraph, we will examine the dependence of the ring patterns on conditions including the type of solvents, liquid temperature, and the duration and frequency of CW beams in order to determine whether SSPM originates from $\chi^{(3)}$ of graphene or simply a thermal lens effect of the solvent.

If the refractive index change comes from the intrinsic $\chi^{(3)}$ of graphene, it should not depend strongly on the type of solvents or solvent temperature. Figure 2a-c show three diffraction patterns with graphene dispersed in NMP, ethanol and DI water when the numbers of rings achieved maximum for each case. At a laser power of 60 mW, similar numbers of diffraction rings are observed in NMP and ethanol, but almost none are observed in water. The laser power must be increased to 500 mW in order to detect similar diffraction patterns in water. Figures 2d-e show the diffraction rings when DI water was kept at three temperatures: 4 °C, 25 °C and 60 °C. It can be seen that the diffraction rings are much fewer at 4 °C than those at higher temperatures. Another distinction between Figure 1 and 2d-e is that the diffraction rings are much more distorted at higher laser powers, due to the laser induced natural convection of the solvent^{14, 15, 17,}

19, 27

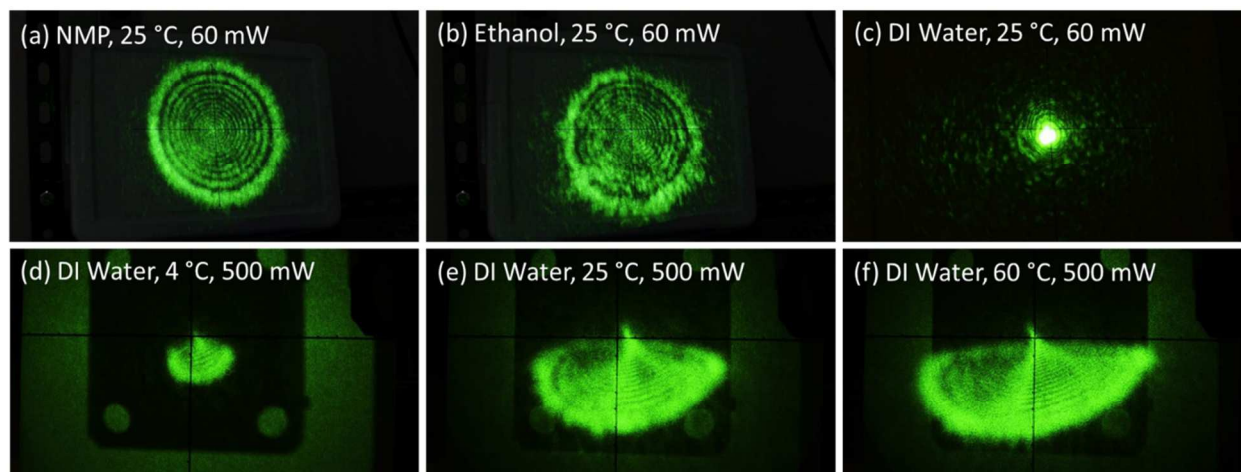


Figure 2. Dependence of diffraction rings on solvent and solvent temperature of graphene suspension. (a-c) Graphene suspension in (a) NMP, (b) Ethanol and (c) deionized water. Laser power: 60 mW. Images were captured when the patterns expanded to the maximum. (d-f) Graphene suspension in deionized water at (d) ~ 4 °C, (e) ~ 20 °C and (f) ~ 60 °C. Laser power: 500 mW. Images were captured after the patterns were stabilized.

The strong dependence of the diffraction ring patterns on the type of solvents and the temperature of water indicates that the change of refractive index might not come from the high $\chi^{(3)}$ of graphene. To find out the effect of $\chi^{(3)}$ on the SSPM, we used graphene oxide suspension for comparison, and the results are shown in Figure 3a-b. Despite a much lower electron density and electron mobility as well as a drastically different band structure^{20, 45}, graphene oxide exhibits a similar number of diffraction rings. Additional experiments were conducted for other nanomaterials, including conductive Au nanoparticles and insulating Co_3O_4 nanoparticles, and similar number of diffraction rings can also be observed under the same conditions. These observations imply that SSPM has little to do with the electronic and optical properties of the nanomaterials.

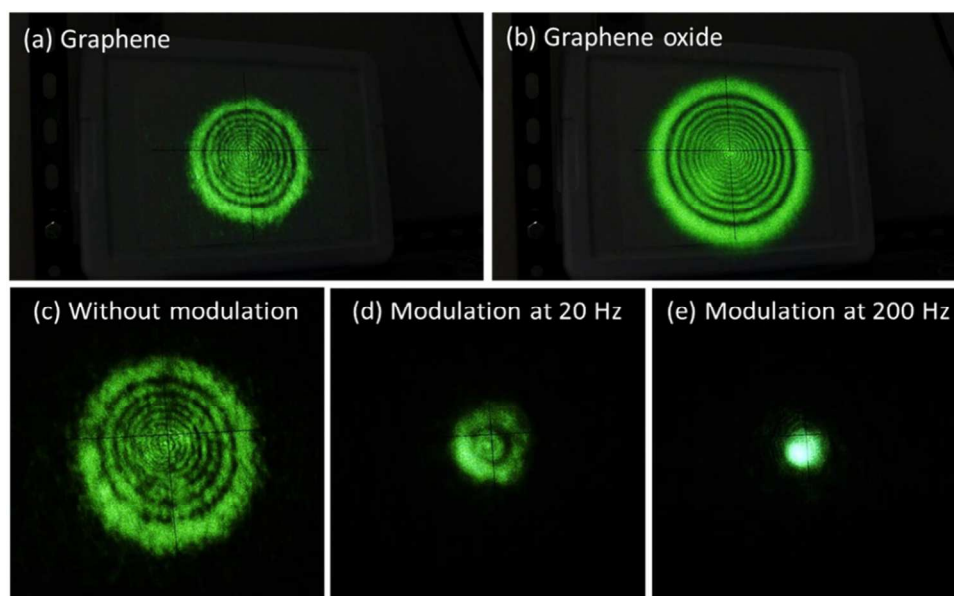


Figure 3. (a-b) Diffraction ring patterns with (a) graphene suspension and (b) graphene oxide suspension in NMP. (c-e) Diffraction ring patterns with graphene suspension in NMP (c) without laser modulation, (d-e) with modulation at (b) 20 Hz and (c) 200 Hz. Laser power: 40 mW. Images were captured when the pattern expanded to the maximum.

It is now clear that the observed diffraction patterns are not due to the unique properties of graphene, but it still remains elusive whether they are caused by nonlinear $\chi^{(3)}$ optics or the thermal lens effect. To distinguish these two effects, we performed two additional control experiments. Figure 3c-d show the diffraction rings when a mechanical chopper is used to modulate the intensity of the CW laser beam. The idea is to keep the magnitude of the electrical field of the laser beam constant, while reducing the duration of CW beam. The number of diffraction rings decreases significantly when the beam is modulated at 20 Hz, and no rings can be observed at 200 Hz. If SSPM is a $\chi^{(3)}$ nonlinear optical effect, the diffraction rings should remain constant regardless of the CW laser modulation. The electronic or nonlinear $\chi^{(3)}$ optical response of a material is on the order of sub-picoseconds, much shorter than the duration of modulated CW laser and the transient thermal lens effect^{7, 23, 46}.

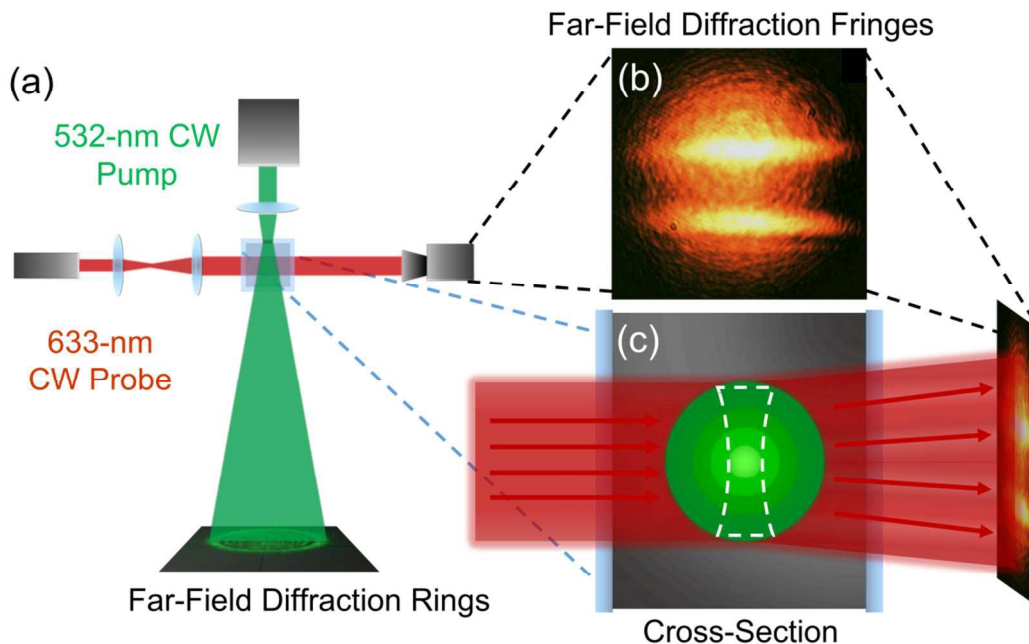


Figure 4. Using a 633-nm 10-mW CW laser to probe the relative change in refractive index of the suspension induced by a 532-nm 500-mW laser beam. (a) Experimental configuration. (b-c) Diffraction pattern of the 633-nm laser beam with graphene in DI water.

The disproof of the $\chi^{(3)}$ effect is further supported by directly probing the refractive index change induced by the laser beam⁴³. Figures 4a-c show the experimental setup and diffraction of a weaker 633-nm probe laser. The effect of convection and solvent on the diffraction of the probe laser beam is similar to those observed in self-diffraction in Figure 2. If it is a $\chi^{(3)}$ effect, the refractive index in the beam path should be larger than the surrounding liquid with the maximum in the beam center, i.e., the beam path will behave as a positive cylindrical lens for the probe laser. On the contrary, the beam path will become a negative cylindrical lens if it is a thermal lens effect of the solvent because the index decreases when the solvent temperature increases. The relative lower intensity in the center of the diffracted beam indicates a lower refractive index, confirming that it is a thermal lens effect of the liquid⁴³.

We can conclude now that it is the temperature dependent refractive index of the solvent rather than the nonlinear refractive index n_2 of graphene or GO that is responsible for the SSPM. Similar thermal lens effect has been observed in solutions of absorbing molecules and can be qualitatively explained based on the laser induced local heating and temperature dependent refractive index, i.e., thermal optic coefficient^{27, 43}. When a solvent expands, its density will reduce, so does the refractive index. The transition from ordinary transmission to the full formation of diffraction rings is the time for 2D materials to absorb and convert laser light to thermal energy and then transfer the thermal energy to the solvent and establish a spatial temperature gradient. Because a temperature gradient will create fluid convection, a stable temperature distribution and flow pattern are established only when the incident laser power and thermal dissipation through thermal conduction and convection are balanced. The convection will reduce temperature gradient above the laser spot, resulting in the squeezed diffraction rings noted earlier. The reduced laser heating time and average laser power decreases the temperature gradient in Figure 3d-e, leading to reduced number of diffraction rings. The reason why water requires higher laser power than ethanol and NMP to produce similar phase shift is because water has a larger thermal capacity and higher thermal conductivity (see Table S1, Fig. S5). A unique feature of water is that its density reaches the maximum at 4 °C, consequently, its thermal-optic coefficient decreases when temperature drops and becomes zero at this temperature⁴⁷, which explains very few diffraction rings at low temperature in Figure 2. Compared with graphene, graphene oxide has less thermal conductivity; furthermore, GO solution has a higher viscosity than graphene suspension due to GO's hydrophilicity as opposed to hydrophobicity of graphene. Lower thermal conductivity and high viscosity makes local

temperature higher in GO solution and thus more number of diffraction rings than that in graphene suspension, as shown in Figure 3b^{48, 49}.

To obtain a quantitative understanding of the relationship between laser power and diffraction ring numbers, we used commercial computational fluid dynamics and performed numerical simulations of laser induced spatial temperature field. Due to the dilute concentrations of graphene, its effects on the thermophysical properties of the solvent, such as density, thermal conductivity, specific heat and viscosity, are negligible. The time for heat transfer from graphene to the surrounding solvent after the optical absorption is also not considered since it is almost instantaneous due to the extremely small thermal mass of the graphene flakes. Figure 5 shows the simulated temperature fields in three graphene suspensions after a laser illumination of 0.4 and 4 seconds, respectively. It is clear that at 0.4 seconds, the temperature fields are represented by a series of contour lines that are concentric with the incident laser spot, indicating that heat transfer is uniform in all directions and that the dominant heat transfer mode is thermal conduction. At 4 seconds, however, the temperature contours clearly shift upward and the difference between the center and peripheral increases, which resembles the typical buoyant plume structure in natural convection⁴⁷. The laser induced local temperature gradient is least pronounced in water suspension of graphene due to the fact that water has higher specific heat, higher thermal conductivity, and lower thermal expansion. Temperature gradients in ethanol and NMP are quite similar because they have the similar thermal dynamic properties.

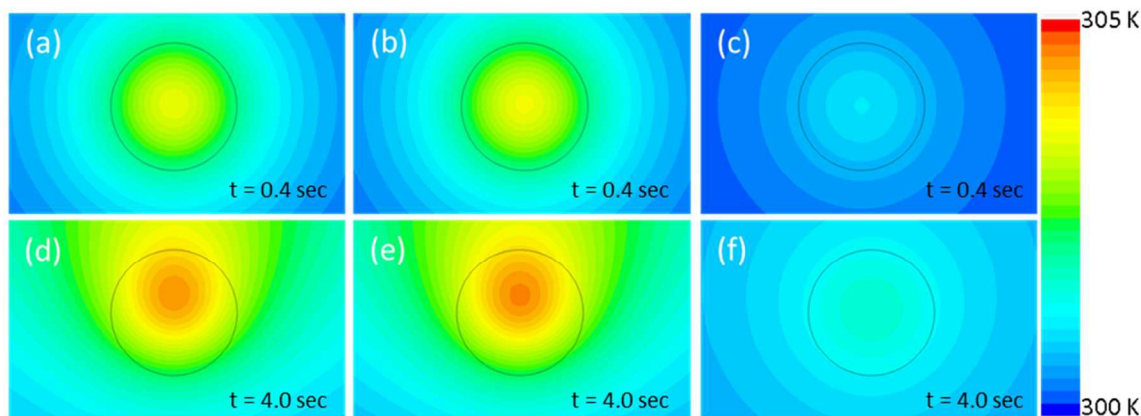


Figure 5. Simulation of flow temperature distribution of graphene in ethanol (a, d), graphene in NMP (b, e), and graphene in Water (c, f) at illumination time of 0.4 sec (a-c) and 4.0 sec (d-f). Black circles indicate the laser spots with 200 μm in diameter

Based on the temperature distribution obtained above and the thermal-optic coefficient of solvents, the local refractive index of the fluid and the total phase shift experienced by the laser beam can be calculated. Then, by using the Fresnel–Kirchhoff diffraction integral, the far-field Fraunhofer diffraction pattern is obtained^{9, 27}. Because a similar detailed calculation of diffraction pattern has been reported, here we try to understand the main feature of diffraction rings²⁷. First, the diffraction pattern is just the Fourier transformation of the phase retardation plane created by temperature distribution^{9, 27}. Cylindrical phase planes in Figure 5a-b lead to symmetrical ring patterns in Figure 2a-b when convection is weak. Elongated phase shift in Figure 5d-e results in squeezed rings in Figure 1 at 1 second in the upper space of the laser beam. Secondly, the total number of diffraction rings can be estimated from the total phase shift in multiples of 2π . For example, for ethanol in Figure 5a, the temperature between the center and peripheral of the laser beam is about 2 degrees, equivalent to 15 times of 2π . This number agrees roughly with 13 rings in Figure 2b.

Apparently the well-accepted $\chi^{(3)}$ (10^{-7} esu) was used to estimate the total phase shift and explain the observed diffraction rings^{13-15, 23}. There must be something wrong with their calculations, and careful examination reveals two major mistakes: the use of cuvette length as the nonlinear optical path length and the conversion between nonlinear index n_2 and $\chi^{(3)}$. Let's take our case for example. The number of graphene layers is about 90 based on 10-12% optical transmission and 97.7% transmittance of single layer graphene, so the total effective optical path length of graphene is ~ 30 nm instead of 1 cm, the optical length of the cuvette¹³⁻¹⁵. This is a large error off by five orders of magnitude. Based on $\chi^{(3)}$ versus n_2 conversion^{23, 50-52}, we obtain a $n_2 \sim 10^{-9}$ cm²/W⁵², which is four orders of magnitude smaller than previously calculated values although the same $\chi^{(3)}$ was used¹³⁻¹⁵. For a typical CW laser intensity of 100 W/cm², we then obtain a phase shift of $\sim 10^{-7}\pi$, which is totally negligible compared to the thermal lens effect. Ultrafast lasers are required to observe the intrinsic nonlinear effect of graphene⁵². The same estimation can be applied to TMDs, black phosphor and CNTs. Because they have optical absorption coefficients and $\chi^{(3)}$ on more or less the same order of magnitude, it is impossible for them to generate a phase shift that is seven orders of magnitude larger than that of graphene. Thus, we conclude that the same thermal effect is responsible for the observed ring patterns in their liquid suspensions¹⁶⁻²¹.

4. CONCLUSIONS

In summary, a series of generic experiments are designed to distinguish nonlinear optical effect from other mechanisms. The temperature dependent refractive index of the solvents is found to be responsible for large laser induced spatial self-phase modulations and multiple diffraction ring patterns. The thermal lens effect is a natural consequence of optical absorption by 2D

nanomaterials, and can hardly be avoided. Due to the high sensitivity of diffraction rings on solvents, the thermal lens effect can be used to measure their thermal and thermal-optical constants^{48, 49, 53}. An accurate understanding of solvent fluids, suspensions' nanostructures as well as their interaction with light is crucial for new optical and opto-fluidic applications of 2D nanomaterials.

ACKNOWLEDGEMENTS

J.M.B. acknowledges support from the National Science Foundation (Career Award ECCS-1240510) and the Robert A Welch Foundation (E-1728). Y.W. acknowledges support from China Postdoctoral Science Foundation (2015M582535) and the Fundamental Research Funds for Key Universities (ZYGX2015J135).

Electronic Supplementary Material: Supplementary material (SEM and TEM micrographs of graphene flakes; AFM image of graphene oxide; dependence of diffraction ring number on laser power; and parameters for computational fluid dynamics) is available in the online version of this article.

REFERENCES

1. J. B. Gerardo and J. T. Verdeyen, *Appl. Phys. Lett.*, 1963, **3**, 121-123.
2. W. R. Callen, B. G. Huth and R. H. Pantell, *Appl. Phys. Lett.*, 1967, **11**, 103.
3. F. W. Dabby, Gustafso.Tk, J. R. Whinnery, Kohanzad.Y and P. L. Kelley, *Appl. Phys. Lett.*, 1970, **16**, 362.
4. J. P. Gordon, R. C. C. Leite, R. S. Moore, S. P. S. Porto and J. R. Whinnery, *J. Appl. Phys.*, 1965, **36**, 3.
5. R. Y. Chiao, E. Garmire and C. H. Townes, *Phys. Rev. Lett.*, 1964, **13**, 479-&.
6. P. L. Kelley, *Phys. Rev. Lett.*, 1965, **15**, 1005-&.
7. M. G. Kuzyk, R. A. Norwood, J. W. Wu and A. F. Garito, *J. Opt. Soc. Am. B-Opt. Phys.*, 1989, **6**, 154-164.
8. O. Werner, B. Fischer and A. Lewis, *Opt. Lett.*, 1992, **17**, 241-243.
9. S. D. Durbin, S. M. Arakelian and Y. R. Shen, *Opt. Lett.*, 1981, **6**, 411-413.

10. H. Hsiung, L. P. Shi and Y. R. Shen, *Phys. Rev. A*, 1984, **30**, 1453-1460.
11. A. B. Villafranca and K. Saravanamuttu, *J. Opt. A-Pure Appl. Opt.*, 2009, **11**, 7.
12. A. S. Zolotko, V. F. Kitaeva, N. Kroo, N. N. Sobolev and L. Chillag, *Jetp Lett.*, 1980, **32**, 158-162.
13. R. Wu, Y. L. Zhang, S. C. Yan, F. Bian, W. L. Wang, X. D. Bai, X. H. Lu, J. M. Zhao and E. G. Wang, *Nano Lett.*, 2011, **11**, 5159-5164.
14. G. Z. Wang, S. F. Zhang, F. A. Umran, X. Cheng, N. N. Dong, D. Coghlan, Y. Cheng, L. Zhang, W. J. Blau and J. Wang, *Appl. Phys. Lett.*, 2014, **104**, 5.
15. Y. L. Wu, L. L. Zhu, Q. Wu, F. Sun, J. K. Wei, Y. C. Tian, W. L. Wang, X. D. Bai, X. Zuo and J. M. Zhao, *Appl. Phys. Lett.*, 2016, **108**, 241110.
16. G. Z. Wang, S. F. Zhang, X. Y. Zhang, L. Zhang, Y. Cheng, D. Fox, H. Z. Zhang, J. N. Coleman, W. J. Blau and J. Wang, *Photonics Res.*, 2015, **3**, A51-A55.
17. Y. L. Wu, Q. O. Wu, F. Sun, C. Cheng, S. Meng and J. M. Zhao, *PNAS*, 2015, **112**, 11800-11805.
18. X. Li, K. Hu, B. Lyu, J. Zhang, Y. Wang, P. Wang, S. Xiao, Y. Gao and J. He, *J. Phys. Chem. C*, 2016, **120**, 18243-18248.
19. W. H. Wang, Y. L. Wu, Q. Wu, J. J. Hua and J. M. Zhao, *Sci Rep*, 2016, **6**, 22072.
20. G. Yang, Y. Zhang and X. Yan, *Journal of Semiconductors*, 2013, **34**, 083004-083008.
21. M. D. Zidan, A. W. Allaf, M. B. Alsous and A. Allahham, *Opt. Laser Technol.*, 2014, **58**, 128-134.
22. F. Bonaccorso, Z. Sun, T. Hasan and A. C. Ferrari, *Nat. Photonics*, 2010, **4**, 611-622.
23. E. Hendry, P. J. Hale, J. Moger, A. K. Savchenko and S. A. Mikhailov, *Phys. Rev. Lett.*, 2010, **105**, 4.
24. Q. L. Bao, H. Zhang, Y. Wang, Z. H. Ni, Y. L. Yan, Z. X. Shen, K. P. Loh and D. Y. Tang, *Adv. Funct. Mater.*, 2009, **19**, 3077-3083.
25. S. Yamashita, *J. Lightwave Technol.*, 2012, **30**, 427-447.
26. J. J. Dean and H. M. van Driel, *Phys. Rev. B*, 2010, **82**, 125411.
27. R. Karimzadeh, *J. Opt.*, 2012, **14**, 9.
28. Y. Han, W. Zhang, F. Dong, Y. Xia, W. Znag, P. Yang, G. Gu, Y. Du and D. Feng, *Chinese Physics Letters*, 1992, **9**, 647.
29. N. Behabtu, J. R. Lomeda, M. J. Green, A. L. Higginbotham, A. Sinitskii, D. V. Kosynkin, D. Tsentlovich, A. N. G. Parra-Vasquez, J. Schmidt, E. Kesselman, Y. Cohen, Y. Talmon, J. M. Tour and M. Pasquali, *Nat. Nanotechnol.*, 2010, **5**, 406-411.
30. T. Z. Shen, S. H. Hong and J. K. Song, *Nat. Mater.*, 2014, **13**, 394-399.
31. C. Zakri, C. Blanc, E. Grelet, C. Zamora-Ledezma, N. Puech, E. Anglaret and P. Poulin, *Philos. Trans. R. Soc. A-Math. Phys. Eng. Sci.*, 2013, **371**.
32. W. Tie, S. S. Bhattacharyya, Y. J. Lim, S. W. Lee, T. H. Lee, Y. H. Lee and S. H. Lee, *Opt. Express*, 2013, **21**, 19867-19879.
33. B. Senyuk, N. Behabtu, A. Martinez, T. Lee, D. E. Tsentlovich, G. Ceriotti, J. M. Tour, M. Pasquali and Smalyukh, II, *Nat. Commun.*, 2015, **6**, 7.
34. V. Nicolosi, M. Chhowalla, M. G. Kanatzidis, M. S. Strano and J. N. Coleman, *Science*, 2013, **340**, 1420.
35. F. Lin, X. Tong, Y. N. Wang, J. M. Bao and Z. M. M. Wang, *Nanoscale Res. Lett.*, 2015, **10**, 16.
36. H. Coles and S. Morris, *Nat. Photonics*, 2010, **4**, 676-685.
37. Y. Huang and A. J. Mason, *Lab Chip*, 2013, **13**, 3929-3934.

38. M. Soltani, J. T. Inman, M. Lipson and M. D. Wang, *Opt. Express*, 2012, **20**, 22314-22326.
39. A. C. Ferrari, F. Bonaccorso, V. Fal'ko, K. S. Novoselov, S. Roche, P. Boggild, S. Borini, F. H. L. Koppens, V. Palermo, N. Pugno, J. A. Garrido, R. Sordan, A. Bianco, L. Ballerini, M. Prato, E. Lidorikis, J. Kivioja, C. Marinelli, T. Ryhanen, A. Morpurgo, J. N. Coleman, V. Nicolosi, L. Colombo, A. Fert, M. Garcia-Hernandez, A. Bachtold, G. F. Schneider, F. Guinea, C. Dekker, M. Barbone, Z. P. Sun, C. Galiotis, A. N. Grigorenko, G. Konstantatos, A. Kis, M. Katsnelson, L. Vandersypen, A. Loiseau, V. Morandi, D. Neumaier, E. Treossi, V. Pellegrini, M. Polini, A. Tredicucci, G. M. Williams, B. H. Hong, J. H. Ahn, J. M. Kim, H. Zirath, B. J. van Wees, H. van der Zant, L. Occhipinti, A. Di Matteo, I. A. Kinloch, T. Seyller, E. Quesnel, X. L. Feng, K. Teo, N. Rupesinghe, P. Hakonen, S. R. T. Neil, Q. Tannock, T. Lofwander and J. Kinaret, *Nanoscale*, 2015, **7**, 4598-4810.
40. L. Q. He, J. Ye, M. Shuai, Z. Zhu, X. F. Zhou, Y. A. Wang, Y. Li, Z. H. Su, H. Y. Zhang, Y. Chen, Z. P. Liu, Z. D. Cheng and J. M. Bao, *Nanoscale*, 2015, **7**, 1616-1622.
41. X. W. He, W. L. Gao, L. J. Xie, B. Li, Q. Zhang, S. D. Lei, J. M. Robinson, E. H. Haroz, S. K. Doorn, W. P. Wang, R. Vajtai, P. M. Ajayan, W. W. Adams, R. H. Hauge and J. Kono, *Nat. Nanotechnol.*, 2016, **11**, 633.
42. X. F. Zhou and Z. P. Liu, *Chem. Commun.*, 2010, **46**, 2611-2613.
43. M. G. Beygi, R. Karimzadeh and M. Dashtdar, *Opt. Laser Technol.*, 2015, **66**, 151-155.
44. J. D. Zhang, X. F. Yu, W. J. Han, B. S. Lv, X. H. Li, S. Xiao, Y. L. Gao and J. He, *Opt. Lett.*, 2016, **41**, 1704-1707.
45. K. P. Loh, Q. L. Bao, G. Eda and M. Chhowalla, *Nat. Chem.*, 2010, **2**, 1015-1024.
46. R. R. Alfano, S. L. Shapiro and L. L. Hope, *Physical Review A*, 1972, **6**, 433.
47. G. Abbate, U. Bernini, E. Ragozzino and F. Somma, *J. Phys. D-Appl. Phys.*, 1978, **11**, 1167-1172.
48. M. Kole and T. K. Dey, *J. Appl. Phys.*, 2013, **113**, 084307.
49. M. Hadadian, E. K. Goharshadi and A. Youssefi, *J. Nanopart. Res.*, 2014, **16**, 2788.
50. R. W. Boyd, Z. M. Shi and I. De Leon, *Opt. Commun.*, 2014, **326**, 74-79.
51. E. Dremetsika, B. Dlubak, S. P. Gorza, C. Ciret, M. B. Martin, S. Hofmann, P. Seneor, D. Dolfi, S. Massar, P. Emplit and P. Kockaert, *Opt. Lett.*, 2016, **41**, 3281-3284.
52. J. B. Khurgin, *Appl. Phys. Lett.*, 2014, **104**, 5.
53. H. Ono and K. Shibata, *Jpn. J. Appl. Phys. Part 1 - Regul. Pap. Short Notes Rev. Pap.*, 2003, **42**, 186-193.